Heterodinuclear Complexes Containing d- and f-block Elements: Synthesis, Structural Characterization, and Metal−Metal Interactions of Novel Chromium(III)−Lanthanide(III) Compounds Bridged by Oxalate

Takayuki Sanada, Takayoshi Suzuki, Takafumi Yoshida, and Sumio Kaizaki*

Department of Chemistry, Graduate School of Science, Osaka University, Toyonaka, 560, Japan

Received December 16, 1997

The reaction of Ln(III) ions with a tripodal ligand $HBpz_3^-$ (hydrotris(pyrazol-1-yl)borate) and a "complex ligand" $[Cr(acac)_2(ox)]^-$ ($acac^-$ = acetylacetonate, ox^{2-} = oxalate) in aqueous solution afforded a series of the novel 3d−4f heterodinuclear complexes $[(acac)_2Cr(ox)Ln(HBpz_3)_2]$ (Ln = Eu (**1**), Gd (**2**), Tb (**3**), Yb (**4**), Lu (**5**)). The crystal structure of **4** has been determined by X-ray diffraction. Complex **4** crystallizes in monoclinic space group $P2/n$, of which the cell parameters are $a = 8.594(3)$ Å, $b = 18.538(4)$ Å, $c = 12.093(2)$ Å, $\beta = 93.71(2)°$, and $Z = 2$. The Yb atom has an eight-coordinate distorted square antiprismatic coordination geometry. The intramolecular Cr···Yb distance is 5.631(1) Å. The magnetic susceptibility data for complex **2** showed that the $Cr^{III}-Gd^{III}$ interaction is weakly antiferromagnetic with an exchange coupling constant $J_{CrGd} = -0.09$ cm^{-1}. The luminescence measurements demonstrated the energy transfers for both Ln(III) → Cr(III) and Cr(III) → Ln(III), of which the degree of emission quenching depends on the energy gap of the excited levels in two metal centers. These results reveal that the metal−metal interactions between Cr(III) and Ln(III) are very weak in magnetic interaction but are strong from the viewpoint of energy transfer.

Introduction

A large number of heteropolymetallic compounds have been investigated[1] from a unique physicochemical point of view arising from metal−metal interactions. As models for novel magnetic materials, especially concerning high-temperature superconducting ceramics, much attention has been paid to heteropolymetallic compounds including both transition metal ions [Cr(III),[2] Fe(II),[3] Co(II),[4] Ni(II),[5] Cu(II),[6−9] Zn(II)[10]] and lanthanide ions. Very recently we succeeded in synthesizing new 3d−4f heterotrinuclear complexes, $[NiL\{Ln(HBpz_3)_2\}_2]$ [L = 1,3-trimethylenebis(oxamidate) or 1,2-ethylenebis(oxamidate), $HBpz_3^-$ = hydrotris(pyrazol-1-yl)borate], with novel linear $Ln^{III}-Ni^{II}-Ln^{III}$ structures.[11] In this case, there is no magnetic interaction between the square planar diamagnetic Ni(II) and paramagnetic Ln(III). Further, a magnetic study of the VO^{2+}−Gd(III) dinuclear complex has recently been communicated.[12] The simplicity of the magnetic properties of Gd(III) ion facilitates examinations of the 3d−4f magnetic interactions for discrete transition metal ion−Gd(III) dinuclear complexes.[6−9,12] These magnetic interactions between the transition metal ion and Gd(III) are found to be weakly ferromagnetic in which J values are usually less than 10 cm^{-1}.[6−9,12] From the viewpoint of energy transfer, however, Eu(III) emissions decrease drastically due to the energy transfer from the excited 4f to 3d center.[13] However, there are no studies on the reverse 3d → 4f energy transfer or on the effect of the lanthanide ions in the

* Corresponding author. E-mail: kaizaki@chem.sci.osaka-u.ac.jp.

(1) (a) Kahn, O. *Struct. Bonding (Berlin)* **1987**, *68*, 89. (b) Kahn, O. *Molecular Magnetism*; VCH: Weinheim, 1993.
(2) (a) Sakagami, N.; Tsunekawa, M.; Konno, T.; Okamoto, K. *Chem. Lett.* **1997**, 575. (b) Sakagami, N.; Okamoto, K. *Chem. Lett.* **1998**, 201 (c) Decurtins, S.; Gross, M.; Schmalle, H. W.; Ferlay, S. *Inorg. Chem.* **1998**, 37, 2443.
(3) (a) Piguet, C.; Rivara-Minten, E.; Bernardinelli, G.; Bünzli, J.-C. G.; Hopfgartner, G. *J. Chem. Soc., Dalton Trans.* **1997**, 421. (b) Piguet, C.; Rivara-Minten, E.; Hopfgartner, G.; Bünzli, J.-C. G. *Helv. Chim. Acta* **1995**, *78*, 1651.
(4) (a) Brechin, E. K.; Harris, S. G.; Parsons, S.; Winpenny, R. E. P. *J. Chem. Soc., Dalton Trans.* **1997**, 1665. (b) Aratake, Y.; Okawa, H.; Asato, E.; Sakiyama, H.; Kodera, M.; Kida, S.; Sakamoto, M. *J. Chem. Soc., Dalton Trans.* **1990**, 2941.
(5) (a) Costes, J.-P.; Dahan, F.; Dupuis, A.; Laurent, J.-P. *Inorg. Chem.* **1997**, *36*, 4284. (b) Yukawa, Y.; Igarashi, S.; Yamano, A.; Sato, S. *J. Chem. Soc., Chem. Commun.* **1997**, 711. (c) Archibald, S. J.; Blake, A. J.; Parsons, S.; Schröder, M.; Winpenny, R. E. P. *J. Chem. Soc., Dalton Trans.* **1997**, 173. (d) Goodgame, D. M. L.; Menzer, S.; Ross, A. T.; Williams, D. J. *J. Chem. Soc., Chem. Commun.* **1994**, 2605.
(6) (a) Andruh, M.; Ramade, I.; Codjovi, E.; Guillou, O.; Kahn, O.; Trombe, J. C. *J. Am. Chem. Soc.* **1993**, 115, 1822. (b) Oushoorn, R. L.; Boubekeur, K.; Batail, P.; Guillou, O.; Kahn, O. *Bull. Soc. Chim. Fr.* **1996**, *133*, 777. (c) Ramade, I.; Kahn, O.; Jeannin, Y.; Robert, F. *Inorg. Chem.* **1997**, *36*, 930.
(7) (a) Blake, A. J.; Gould, R. O.; Grant, C. M.; Milne, P. E. Y.; Parsons, S.; Winpenny, R. E. P. *J. Chem. Soc., Dalton Trans.* **1997**, 485. (b) Sanz, J. L.; Ruiz, R.; Gleizes, A.; Lloret, F.; Faus, J.; Julve, M.; Borras-Almenar, J. J.; Journaux, Y. *Inorg. Chem.* **1996**, *35*, 7384. (c) Chen, X. M.; Wu, Y. L.; Tong, Y. X.; Huang, X. Y. *J. Chem. Soc., Dalton Trans.* **1996**, 2443. (d) Chen, X. M.; Tong, M. L.; Wu, Y. L.; Luo, Y. J. *J. Chem. Soc., Dalton Trans.* **1996**, 2181.
(8) (a) Costes, J.-P.; Dahan, F.; Dupuis, A.; Laurent, J.-P. *Inorg. Chem.* **1997**, *36*, 3429. (b) Ramade, I.; Kahn, O.; Jeannin, Y.; Robert, F. *Inorg. Chem.* **1997**, *36*, 930. (c) Costes, J.-P.; Dahan, F.; Dupuis, A.; Laurent, J.-P. *Inorg. Chem.* **1996**, *35*, 2400.
(9) (a) Sakamoto, M.; Kitakami, Y.; Sakiyama, H.; Nishida, Y.; Fukuda, Y.; Sakai, M.; Sadaoka, Y.; Matsumoto, A.; Okawa, H. *Polyhedron* **1997**, *16*, 3345. (b) Sakamoto, M.; Nishida, Y.; Ohhara, K.; Sadaoka, Y.; Matsumoto, A.; Okawa, H. *Polyhedron* **1995**, *14*, 2505. (c) Li, Y. T.; Jiang, Z. H.; Ma, S. L.; Li, X. Y.; Liao, D. Z.; Yan, S. P.; Wang, G. L. *Polyhedron* **1994**, *13*, 475.
(10) (a) Piguet, C.; Rivara-Minten, E.; Hopfgartner, G.; Bünzli, J.-C. G. *Helv. Chim. Acta* **1995**, *78*, 1541. (b) Piguet, C.; Hopfgartner, G.; Williams, A. F.; Bünzli, J.-C. G. *J. Chem. Soc., Chem. Commun.* **1995**, 491. (c) Piguet, C.; Bernardinelli, G.; Bünzli, J.-C. G.; Petoud, S.; Hopfgartner, G. *J. Chem. Soc., Chem. Commun.* **1995**, 2575.
(11) Sanada, T.; Suzuki, T.; Kaizaki, S. *J. Chem. Soc., Dalton Trans.* **1998**, 959.
(12) Costes, J.-P.; Dupuis, A.; Laurent, J.-P. *J. Chem. Soc., Dalton. Trans.* **1998**, 735.

S0020-1669(97)01568-1 CCC: $15.00
Published on Web 08/20/1998

complexes excluding a few reports[14] for the doped glasses. To examine these subjects, $Cr^{III}-Ln^{III}$ dinuclear complexes are suitable because Cr(III) usually displays a relative intense luminescence which may exhibit the 3d → 4f energy transfer. No discrete $Cr^{III}-Ln^{III}$ dinuclear complexes have been studied so far, though there have been only a few reports[2] on poly- and tetranuclear structures with light lanthanide ions.

For the synthesis of discrete heterodinuclear complexes, the "complex ligand" method is appropriate, e.g., with use of a $[Cr(acac)_2(ox)]^-$ having one free O−O site, as actually demonstrated in our recent study,[11] where a series of stable 3d−4f complexes containing the $\{Ln(HBpz_3)_2\}^+$ moiety could be prepared introducing the concept that O−O didentate uninegative coligands complete the coordination sphere of the lanthanide ions as reported by Moss and Jones.[15] This paper describes the successful synthesis of a series of novel 3d−4f heterodinuclear complexes, $[(acac)_2Cr(ox)Ln(HBpz_3)_2]$ (Ln = Eu (**1**), Gd (**2**), Tb (**3**), Yb (**4**), Lu (**5**)). Particular attentions is focused on the crystal structure of complex **4** and the metal−metal interactions from two viewpoints: the magnetic interaction and the energy transfer between the Cr(III) and Ln(III).

Experimental Section

Synthesis. All chemicals were reagent grade and used as received. Lanthanide trichloride hexahydrates (Ln = Eu, Tb, Yb) and triacetate tetrahydrates (Ln = Gd, Lu) were purchased from Wako Pure Chemical Industries Ltd. Potassium hydrotris(pyrazol-1-yl)borate was prepared by the literature method.[16]

$Na[Cr(acac)_2(ox)]\cdot H_2O$. To an aqueous solution (60 cm^3) of $CrCl_3\cdot 6H_2O$ (1.19 g, 5 mmol) and $K_2C_2O_4\cdot H_2O$ (0.92 g, 5 mmol) was added a mixture of acetylacetone (Hacac) (1.00 g, 10 mmol) and KOH (0.56 g, 10 mmol) in water (60 cm^3). The mixed solution became cloudy. This was heated at 60 °C for 30 min with stirring, until the solution became clear while forming insoluble red crystals $[Cr(acac)_3]$. After cooling to room temperature, they were filtered off. The filtrate was poured into a column of QAE-Sephadex (A-25, Cl^- form) ion exchanger. Elution with 0.1 mol·dm^{-3} NaCl solution gave a purple band of a uninegative complex, leaving slower moving bands. The purple eluate was concentrated to dryness by a rotatory evaporator. A purple powder was dissovled in methanol, and the white residue(sodium chloride) was removed by filtration. This was repeated a few times. The complete removal of NaCl was accomplished by passage through a Sephadex G-10 column. A purple powder was obtained by condensing the elaute to dryness by a rotatory evaporator. Yield: 0.57 g (30%). Anal. Calcd for $C_{12}H_{16}CrNaO_9$: C, 38.00; H, 4.26. Found: C, 37.30; H, 4.17.

$[(acac)_2Cr(ox)Ln(HBpz_3)_2]$ (Ln = Eu (1), Gd (2), Tb (3), Yb (4), Lu (5)). Each aqueous solution of $Na[Cr(acac)_2(ox)]\cdot H_2O$ (0.076 g, 0.2 mmol, 10 cm^3) and $K(HBpz_3)$ (0.100 g, 0.4 mmol, 10 cm^3) was added to a stirred aqueous solution of $LnCl_3\cdot 6H_2O$ (Ln = Eu, Tb, Yb) or $Ln(CH_3CO_2)\cdot 4H_2O$ (Ln = Gd, Lu) (0.2 mmol, 15 cm^3). The stirring was allowed to continue for 5 min, and then the mixture was cooled in a refrigerator overnight. The purple precipitate was filtered off, washed with water three times, and dried under vacuum. The crude product was recrystallized from dichloromethane−hexane solution several times.

Measurements. Infrared spectra, UV/vis absorption spectra, and FAB mass spectra, were recorded on a Shimadzu IR-435 spectrophotometer using Nujol mulls, a Perkin-Elmer Lambda19 UV/vis/NIR spectrophotometer, and a JEOL JMS−SX102 mass spectrometer, respectively. Magnetic susceptibility data were collected on microcrystalline samples of the complexes with use of a SQUID-based sample magnetometer on a QUANTUM Design model MPMS instrument. All data were corrected for ligands diamagnetic susceptibilities estimated from Pascal's constants.

Luminescence spectra were recorded using a Perkin-Elmer LS50B spectrophotometer at room temperature and 77 K, using an excitation slit width of 15 nm and an emission slit width of 10 nm with microcrystalline samples. Phosphorescence lifetimes (τ) were measured with the instrument in time-resolved mode and were the average of at least three independent measurements which were made by monitoring the decay at a wavelength corresponding to the maximum intensity of the emission spectrum. The intensity of the emission after the pulsed excitation was monitored after 20 different delay times.

Crystallography. A purple plate crystal (0.48 × 0.24 × 0.08 mm) of complex **4**, which was obtained by slowly evaporating the complex solution in a mixture of chloroform and *n*-hexane, was glued on top of a glass fiber and coated with a thin layer of epoxy resin. The X-ray intensities were measured at 23 °C with graphite-monochromated Mo Kα radiation (λ = 0.710 73 Å) on a Rigaku four-circle diffractometer AFC-5R. The $2\theta-\omega$ scan technique was employed at a scan rate of 8° min^{-1} in θ and scan widths of 1.42 + 0.5 tan θ. Final lattice constants were determined by least-squares refinements of the orientation angles of 25 centered reflections in the range $29 \le 2\theta \le 30°$. Three standard reflections were monitored every 150 reflections and showed no serious decomposition $[|F_o|/(|F_o|)_{initial} > 99\%]$. The intensities collected for ($-h, +k, \pm l$) octants at $2\theta \le 60°$ were corrected for Lorentz−polarization effects, and absorption corrections were made by the Gauss numerical integration method.[17] The observed independent reflections with $I > 3\sigma(I)$ were used for the structural calculations. Systematic absences ($h0l$: $k + l$ odd) indicated the space group *Pn* or *P*2/*n*. Assuming the centrosymmetric space group *P*2/*n* the structure could be solved reasonably by the usual heavy-atom method using SHELXS-86 program.[18] There was a crystallographically imposed C_2 axis, on which the Cr and Yb atoms were located. The positions of hydrogen atoms were obtained by subsequent Fourier-difference syntheses. The function, $\Sigma w(|F_o| - |F_c|)^2$ where $w^{-1} = \sigma^2(F_o) + (0.015|F_o|)^2$, were minimized (refined on *F*) by the full-matrix least-squares method using anisotropic and isotropic thermal parameters for all non-hydrogen and hydrogen atoms, respectively. Complex neutral atom scattering factors were used.[19] All calculation were carried out on an SGI Indy workstation using TEXSAN software.[20]

Results and Discussion

Preparation and Characterization. The elemental analyses data and the characteristic IR bands for the new complexes are summarized in Table 1. The elemental analyses show that the complexes **1**−**5** have the chemical formula consisting of $[Cr(acac)_2(ox)]^-$ and $[Ln(HBpz_3)_2]^+$ with 1:1 ratio. All of the new complexes give almost the identical IR spectra with strong carbonyl stretching bands. These bands were shifted by ca. 20 cm^{-1} to lower frequencies as compared with the carbonyl stretching band at 1690 cm^{-1} for $Na[Cr(acac)_2(ox)]\cdot H_2O$. This fact is attributed to the coordination of the carbonyl oxygens of the oxalato to the metal ions[21] and lanthanide ions.[2b] This carbonyl stretching band shifts to higher frequency with

(13) (a) Sakamoto, M.; Hashimura, M.; Matsuki, K.; Matsumoto, A.; Okawa, H. *Chem. Lett.* **1991**, 1007. (b) Sakamoto, M.; Hashimura, M.; Nakayama, Y.; Matsumoto, A.; Okawa, H. *Bull. Chem. Soc. Jpn.* **1992**, *65*, 1162. (c) Sakamoto, M.; Ohsaki, M.; Yamamoto, K.; Nakayama, Y.; Matsumoto, A.; Okawa, H. *Bull. Chem. Soc. Jpn.* **1992**, *65*, 2514.

(14) Reisfeld, R.; Jørgensen, C. K. *Lasers and Excited States of Rare Earths, Inorganic Chemistry Concepts*; Springer-Verlag: Berlin, 1977; Vol. 1, Chapter 4, pp 157−198.

(15) (a) Moss, M. A. J.; Jones, C. J. *J. Chem. Soc., Dalton Trans.* **1990**, 581. (b) Moss, M. A. J.; Jones, C. J.; Edwards, A. J. *J. Chem. Soc., Dalton Trans.* **1989**, 1393.

(16) Trofimenko, S. *J. Am. Chem. Soc.* **1967**, *89*, 3170.

(17) Busing, W. L.; Levy, H. A. *Acta Crystallogr.* **1957**, *10*, 180.

(18) Sheldrick, G. M. *SHELXS-86: Program for Crystal Structure Determination*; University of Göttingen: Germany, 1986.

(19) Cromer, D. T.; Waber, J. T. *International Tables for X-ray Crystallography*; The Kynoch Press: Birmingham, England, 1974; Vol. 4.

(20) *TEXSAN: Single-Crystal Structure Analysis Software*, Version 1.7; Molecular Structure Corporation: The Woodlands, TX, 1995.

(21) Ohba, M.; Tamaki, H.; Matsumoto, N.; Okawa, H. *Inorg. Chem.* **1993**, *32*, 5385.

Table 1. Elemental Analyses and IR Spectral Data for the Complexes[a]

complex (Ln)	yield (%)	elemental analysis (%) C	H	N	IR/cm^{-1} ν(B−H)	ν(C═O)
1 (Eu)	11	39.37 (39.32)	3.82 (3.75)	18.03 (18.35)	2446	1665
2 (Gd)	18	38.88 (39.09)	3.78 (3.73)	17.97 (18.24)	2444	1666
3 (Tb)	16	38.45 (39.02)	3.67 (3.72)	17.64 (18.21)	2445	1669
4 (Yb)	25	38.28 (38.44)	3.59 (3.66)	17.66 (17.93)	2449	1671
5 (Lu)	27	38.26 (38.36)	3.62 (3.65)	17.61 (17.90)	2450	1672

[a] Calculated values are given in parentheses.

Table 2. FAB Mass Spectral Data for **1** and **5**[a]

complex	*m*/*z*	relative intensity	fragment[b]
1 (Eu)	916 (916)	0.3	$[M - H]^+$
	850 (850)	6.5	$[M - pz]^+$
	818 (818)	1.1	$[M - acac]^+$
	704 (704)	1.7	$[M - HBpz_3]^+$
	579 (579)	100	$[Eu(HBpz_3)_2]^+$
5 (Lu)	940 (940)	1.7	$[M+H]^+$
	872 (872)	16.6	$[M - pz]^+$
	840 (840)	2.2	$[M - acac]^+$
	773 (773)	2.1	$[M - acac - pz]^+$
	726 (726)	8.4	$[M - HBpz_3]^+$
	602 (601)	100	$[Lu(HBpz_3)_2]^+$

[a] Calculated values are given in the parentheses. [b] $M = [(acac)_2Cr(ox)Ln(HBpz_3)_2]$ [Ln = Eu(III) or Lu(III)].

Table 3. UV/Vis Spectral Data for the "Complex Ligand" and Dinuclear Complexes

complex[a]	λ_{max}/nm (ϵ) CT and/or intraligand	d−d		f−f	
$[Cr(acac)_2(ox)]^-$	328 (13 200)	388 (270)	563 (70)		
1 (Eu)	332 (14 200)	394 (390)	569 (71)		
2 (Gd)	332 (12 800)	392 (370)	568 (69)		
3 (Tb)	332 (12 400)	392 (350)	567 (65)		
4 (Yb)	332 (13 500)	392 (380)	568 (76)	930 (3)	975 (10)
5 (Lu)	332 (12 800)	392 (350)	569 (74)		

[a] "Complex ligand", $[Cr(acac)_2(ox)]^-$, was measured in methanol, and dinuclear complexes, **1**−**5**, in dichloromethane solution.

increasing the atomic numbers. This shift results from the lanthanide contraction. In addition, the FAB mass data for **1** and **5** (Table 2) confirm the formation of anhydrous dinuclear complexes $[(acac)_2Cr(ox)Ln(HBpz_3)_2]$ in view of the observation of high mass fragments corresponding to the 3d−4f heterodinuclear complexes.

These complexes were formed readily in an aqueous solution containing 1:1:2 mixtures of Ln^{3+}, $[Cr(acac)_2(ox)]^-$, and $HBpz_3^-$ ions, respectively. The crude precipitates dissolve freely in dichloromethane and chloroform, are sparingly soluble in acetone and acetonitrile, but are insoluble in water, alcohol, and *n*-hexane. They were recrystallized from dichloromethane−hexane solution. The larger the ionic radius of the lanthanide(III), the poorer the yields of the products become. This is because the larger Ln(III) ions tend to form $[Ln(HBpz_3)_3]$ and/or $[\{Ln(HBpz_3)_2\}_2(ox)]$ more readily.

Comparison of the UV/vis absorption spectral data in Table 3 shows almost the same pattern for the five dinuclear complexes **1**−**5**. The first ligand field band corresponding to the $^4T_2 \leftarrow {}^4A_2$ transition of Cr(III) is shifted slightly from 563 nm for $[Cr(acac)_2(ox)]^-$ to 568 ± 1 nm for **1**−**5**. This indicates little structural change of the Cr(III) moiety in the dinuclear

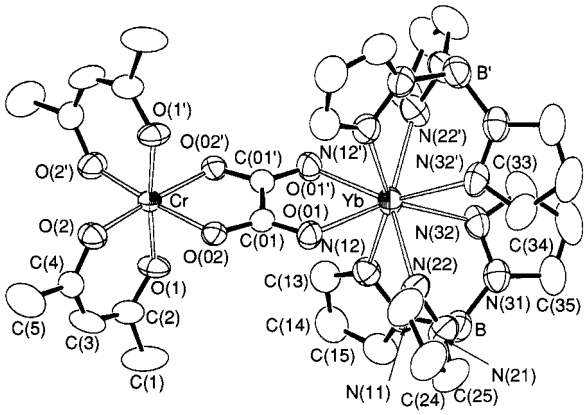

Figure 1. Molecular structure of complex **4** in the crystal, showing 50% probability ellipsoids and the atom labeling scheme.

Table 4. Crystallographic Data for $[(acac)_2Cr(ox)Yb(HBpz_3)_2]$ (**4**)

$C_{30}H_{34}B_2CrN_{12}O_8Yb$	$M = 937.33$
monoclinic	space group $P2/n$
$a = 8.594(3)$ Å	$T = 296.2$ K
$b = 18.538(4)$ Å	$\lambda = 0.710\ 73$ Å
$c = 12.093(2)$ Å	$\rho_{calc.} = 1.619$ g cm^{-3}
$\beta = 93.71(2)°$	$\mu = 27.63$ cm^{-1}
$V = 1922.6(8)$ Å^3	$R = 0.033$[a]
$Z = 2$	$R' = 0.040$[a]

[a] R factors defined as follows: $R = \sum||F_o| - |F_c||/\sum|F_o|$, $R' = [\sum(|F_o| - |F_c|)^2/\sum w|F_o|^2]^{1/2}$, $w^{-1} = \sigma^2(F_o) + (0.015|F_o|)^2$.

complexes. In addition to the CT and/or intraligand and d−d transitions, the f−f band of Yb(III) is observed at 975 nm together with a small peak at 930 nm in **4**. Such a splitting is observed for mononuclear $[Yb(HBpz_3)_2L]$ (e.g. L = acac$^-$) but not for Yb(III) aquo complex ion[22] at room temperature. Therefore, this arises from the sublevels of the $^2F_{5/2}$ term of Yb(III)[23] but not from the magnetic exchange interaction with Cr(III).

Crystallographic Studies. The complex **4** crystallizes to form purple monoclinic plates of space group $P2/n$. The molecular structure is illustrated in Figure 1 with the numbering scheme. Primed atoms are related to their unprimed equivalents with the 2-fold axis through the Cr atom and Yb atom. Crystallographic data for the complex **4** are summarized in Table 4. The selected bond lengths and angles are listed in Table 5.

The Cr atom is located in a distorted octahedral environment with six oxygens which consist of two oxygens from the oxalato ligand and four from two acetylacetonato ligands. The bond length of Cr−O(ox) [2.013(3) Å] is similar to those [2.065(9) and 1.997(7) Å] for the $[Nd\{(eddp)Cr(ox)\}_3(H_2O)_3]\cdot 12H_2O$ (eddp = ethylenediamine-*N*,*N*′-dipropionate)[2b] and [Cr(salen)-(ox)Cu(acpy)] [salen = *N*,*N*′-ethylenebis(salicylideneaminate, acpy = *N*-acetylacetonylidene-*N*-(2-pyridylethyl)aminate][21] but is longer than the Cr−O(ox) (average 1.974(6) Å) in $[CeCr(ox)_3(H_2O)_4]_2\cdot 12H_2O$[2c] and the Cr−O(acac) [1.939(3) Å for Cr−O(1) and 1.927(3) Å for Cr−O(2)]. The bite angle of O(02)−Cr−O(02′) [82.2(2)°] for the five-membered oxalato chelate is smaller than the bite angles for the six-membered acetylacetonato ligands [91.8(1)°].

(22) Carnall, W. T. In *Handbook on the Physics and Chemistry of Rare Earths;* Gschneidner, K. A., Jr.; Eyring, L. R., Eds.; North-Holland Physics Publishing: Amsterdam, 1979; Vol. 3, Chapter 24, pp 171−208.

(23) (a) Ovsyankin, V. V. In *Spectroscopy of Solids Containing Rare Earth Ions;* Kaplyanskii, A. A.; Macfarlane, R. M., Eds.; North-Holland Physics Publishing: Amsterdam, 1987; Chapter 7, pp 343−480. (b) Yatsimirskii, K. B.; Davidenko, N. K. *Coord. Chem. Rev.* **1979**, *27*, 223.

Table 5. Selected Bond Lengths (Å) and Angles (deg) for **4**

Yb−O(01)	2.314(3)	C(01)−C(01′)	1.541(7)
Yb−N(12)	2.469(4)	O(1)−C(2)	1.268(5)
Yb−N(22)	2.400(4)	O(2)−C(4)	1.280(5)
Yb−N(32)	2.473(4)	N(11)−N(12)	1.376(5)
Cr−O(02)	2.013(3)	N(21)−N(22)	1.341(5)
Cr−O(1)	1.939(3)	N(31)−N(32)	1.367(5)
Cr−O(2)	1.927(3)	N(12)−C(13)	1.329(6)
O(01)−C(01)	1.243(4)	N(22)−C(23)	1.350(6)
O(02)−C(01)	1.244(4)	N(32)−C(33)	1.329(6)
O(01)−Yb−O(01′)	70.3(1)	O(02)−Cr−O(02′)	82.2(2)
O(01)−Yb−N(12)	84.1(1)	O(02)−Cr−O(1)	88.2(1)
O(01)−Yb−N(12′)	74.7(1)	O(02)−Cr−O(1′)	87.3(1)
O(01)−Yb−N(22)	72.6(1)	O(02)−Cr−O(2)	93.4(1)
O(01)−Yb−N(22′)	133.9(1)	O(02)−Cr−O(2′)	175.5(1)
O(01)−Yb−N(32)	147.5(1)	O(1)−Cr−O(1′)	174.0(2)
O(01)−Yb−N(32′)	119.2(1)	O(1)−Cr−O(2)	91.8(1)
N(12)−Yb−N(12′)	154.1(2)	O(1)−Cr−O(2′)	92.4(1)
N(12)−Yb−N(22)	75.1(1)	O(2)−Cr−O(2′)	91.0(2)
N(12)−Yb−N(22′)	111.4(1)		
N(12)−Yb−N(32)	70.4(1)	Yb−O(01)−C(01)	118.0(2)
N(12)−Yb−N(32′)	134.4(1)	Cr−O(02)−C(01)	112.5(2)
N(22)−Yb−N(22′)	152.0(2)	O(01)−C(01)−O(02)	126.7(3)
N(22)−Yb−N(32)	81.4(1)	O(01)−C(01)−C(01′)	116.9(2)
N(22)−Yb−N(32′)	75.9(1)	O(02)−C(01)−C(01′)	116.4(2)
N(32)−Yb−N(32′)	71.0(2)		

Table 6. Values of δ and ϕ (deg) for **4**

	idealized polyhedra			
	SAPR	DD	TPRS	**4**
δ_1: O(01)[N(12′)N(22)]N(32′)	0.0	29.5	21.8	8.99
δ_2: O(01′)[N(12)N(22′)]N(32)	0.0	29.5	0.0	8.99
δ_3: O(01)[N(12)N(22)]N(32)	52.5	29.5	48.2	58.10
δ_4: O(01′)[N(12′)N(22′)]N(32′)	52.5	29.5	48.2	58.10
ϕ_1: N(22)−O(01)−O(01′)−N(22′)	24.5	0.0	14.1	27.46
ϕ_2: N(12′)−N(32′)−N(32)−N(12)	24.5	0.0	14.1	23.90

The Yb atom is eight-coordinate with two tridentate $HBpz_3$ ligands and one didentate oxalato ligand. The Yb−O(01) bond length is 2.314(3) Å, which is shorter than the Nd−O(ox) bonds (2.48−2.59 Å) in $[Nd\{(eddp)Cr(ox)\}_3(H_2O)_3]\cdot 12H_2O$[2b] and the Ce−O(ox) bonds (2.595−2.648 Å) in $[CeCr(ox)_3(H_2O)_4]_2\cdot 12H_2O$.[2c] The Yb−N bond lengths range from 2.400(4) to 2.473(4) Å. The bond length of Yb−N(22) [2.400(4) Å] is short, and the other two bond lengths, Yb−N(12) and Yb−N(32) [2.469(4) and 2.473(4) Å, respectively], are similar to each other. The average Yb−N bond length is 2.45 Å compared with 2.44 Å [2.36(1)−2.485(9) Å] for $[Ni(tdo)\{Yb(HBpz_3)_2\}_2]$,[11] 2.43 Å [2.363(6)−2.481(6) Å] for $[Yb(HBpz_3)_2(O_2CPh)]$,[15a] 2.49 Å [2.401(7)−2.601(6) Å] for $[Yb(HBpz_3)_3]$,[24] 2.49 Å [2.432(14)−2.576(11) Å] for $[Yb(HBpz_3)_2(acac)]$,[15b] and 2.48 Å [2.425(12)−2.548(10) Å] for $[Yb(HBpz_3)_2(trop)]$ (Htrop = 2-hydroxycyclohepta-2,4,6-trien-1-one).[15a] The intramolecular Cr···Yb distance is 5.631(1) Å, shorter than the Cr···Nd one (5.876(2) Å) in $[Nd\{(eddp)Cr(ox)\}_3(H_2O)_3]\cdot 12H_2O$[2b] and the Cr···Ce one (5.93 Å) in $[CeCr(ox)_3(H_2O)_4]_2\cdot 12H_2O$.[2c] The intermolecular distances of Cr···Cr, Cr···Yb, and Yb···Yb are 7.209(1), 8.795(1), and 8.594(3) Å, respectively.

The N_6O_2 eight-coordinate geometries [square antiprismatic (SAPR), dodecahedral (DD), and bicapped trigonal prismatic (TPRS)] were examined by using the semiquantitative method of polytopal analysis.[25] The most reasonable geometry around the Yb atom is a square antiprism (SAPR) from the δ and ϕ values as summarized in Table 6. Figure 2 shows a view of the donor atoms perpendicular to the square faces. The δ_1 and δ_2 values showing planarity of the "squares" are both 8.99° in Table 6. In contrast, the δ_1 {O(2)[N(61)N(31)]N(41)} and δ_2 {O(1)[N(11)N(51)]N(21)} values of antiprismatic $[Yb(HBpz_3)_2(trop)]$[15a] are 14.5 and 4.0°. Thus, complex **4** is on a geometric pathway to DD, whereas $[Yb(HBpz_3)_2(trop)]$ is to TPRS. The root-mean-square deviation of the "square" face is 0.081 Å with the largest deviation from the least-squares plane being 0.105 Å for N(32) and N(32′). The dihedral angle of two least-squares planes is 2.38°. The closest apexes of the two squares is composed of the two oxalato oxygen atoms; the O(01)···O(01′) distance is 2.665 Å, which result from the relative short Yb−O bond lengths and the small bite angle of the O(01)−Yb−O(01′). This is contrast to the average distances of N···N and O···N between the two squares, 3.01 and 3.21 Å, respectively.

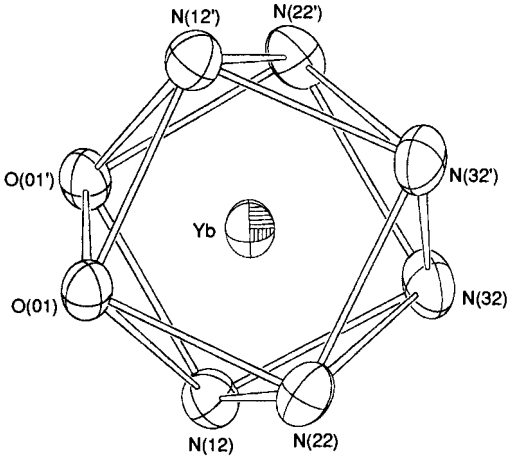

Figure 2. ORTEP drawing showing only the donor atoms coordinating to Yb. The view is perpendicular to one of the "square" faces of the square antiprism coordination geometry (50% probability ellipsoids).

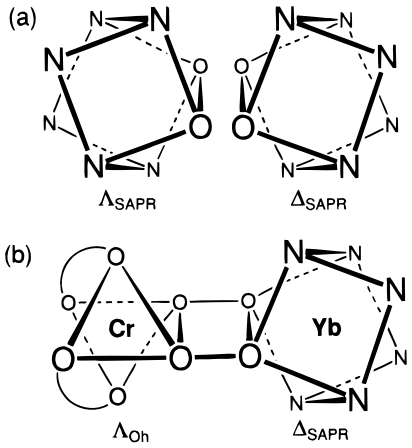

Figure 3. (a) Proposed definition of absolute configuration, Λ_{SAPR} and Δ_{SAPR}, and (b) schematic drawing of complex **4**.

According to the IUPAC definition of the absolute configuration (Λ_{SAPR} and Δ_{SAPR}) around a square antiprismatic metal ion in terms of the skew-line convention as shown in Figure 3a, two molecules in unit cell take $\Lambda_{Oh}-\Delta_{SAPR}$ and $\Delta_{Oh}-\Lambda_{SAPR}$ configurations, as shown in Figure 3b. This result comes from two possibilities: stereospecific formation of only a diastereomeric $\Lambda_{Oh}-\Delta_{SAPR}$ pair and vice versa, or accidental pickup of a crystal of $\Lambda_{Oh}-\Delta_{SAPR}$ and $\Delta_{Oh}-\Lambda_{SAPR}$ pairs from a diastereomeric mixture incorporating $\Lambda_{Oh}-\Lambda_{SAPR}$ and $\Delta_{Oh}-\Delta_{SAPR}$ isomers.

Metal−Metal Interactions. (a) Magnetic Properties. The variable temperature magnetic susceptibilities of the Eu, Tb, Yb, and Lu complexes (**1**, **3**, **4**, and **5**) are shown in Figure 4.

(24) Stainer, M. V. R.; Takats, J. *Inorg. Chem.* **1982**, *21*, 4050.
(25) Drew, M. G. B. *Coord. Chem. Rev.* **1977**, *24*, 179.

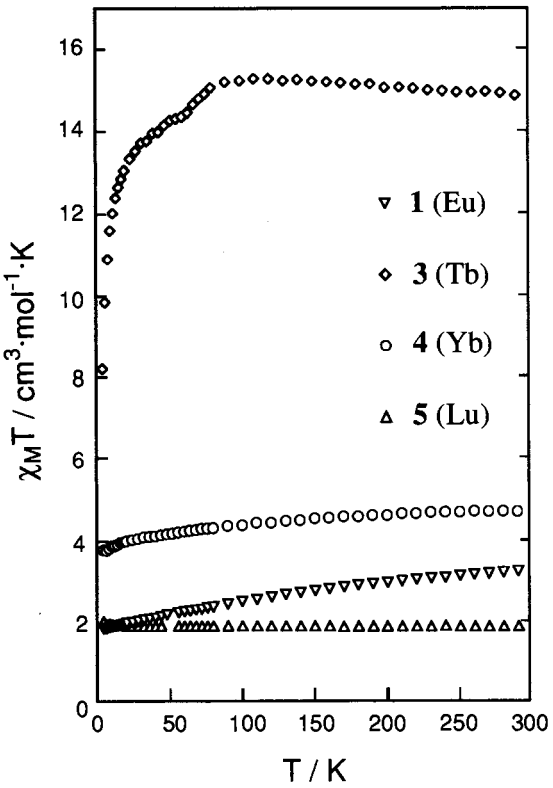

Figure 4. Plots of the $\chi_M T$ versus T for complexes **1**, **3**, **4**, and **5**.

The observed $\chi_M T$ values of these complexes except **1** at room temperature are close to a sum of the values for the uncoupled Cr(III) and Ln(III) systems, where χ_M is the molar magnetic susceptibility per dinuclear complex, the calculated values of **3**, **4**, and **5** being 13.64, 4.45, and 1.88 $cm^3 \cdot mol^{-1} \cdot K$, respectively. The magnetic susceptibility of Eu(III) is expected to be zero in view of the ground $^7F_0$ state, but the observed $\chi_M T$ value of **1** (3.2 $cm^3 \cdot mol^{-1} \cdot K$ at room temperature) is larger than the Cr(III)-only value. This is due to the fact that a certain amount of the magnetic moment is contributed from the excited states $^7F_1$ (ca. 350 cm^{-1}) and $^7F_2$ (ca. 1000 cm^{-1}). The decrease in the $\chi_M T$ values on lowering temperature attributes to the thermal depopulation of these excited levels, leading to the Cr(III)-only value, ca. 1.8 $cm^3 \cdot mol^{-1} \cdot K$ at 4 K. For the Yb complex **4**, the $\chi_M T$ values steadily decrease as T is lowered, giving ca. 3.8 $cm^3 \cdot mol^{-1} \cdot K$ at 4 K. For the Tb complex **3**, the decrease in the $\chi_M T$ values on lowering temperature suggests that there is a relatively strong magnetic interaction between the Cr(III) and Tb(III) ions. Nevertheless, the quantitative analysis of the Tb and Yb complexes must await further detailed examination for the magnetic behavior. The magnetic susceptibility of **5** with a diamagnetic Lu(III) ion is equal to that of the Cr(III) only value. The $\chi_M T$ value slightly increases with lowering temperature, reaching ca. 2.0 $cm^3 \cdot mol^{-1} \cdot K$ at 4 K. This suggests a weak ferromagnetic intermolecular Cr···Cr interaction in **5**.

The magnetic susceptibility data for complex **2** are shown in Figure 5 in the form of the $\chi_M T$ versus T plots. Since the ground state of Gd(III) ($^8S_{7/2}$) is orbitally nondegenerate and well separated from the excited state, Gd(III) gives a simple single ion magnetic properties. There are two possiblities to account for the decreasing behavior of the $\chi_M T$ on lowering temperature. The one is a dominant contribution from the intermolecular interaction. The analysis of the magnetic data was attempted to make in terms of the molecular field approximation[1b,26] including the zero field splitting D. A fitting with $g = 2.00$ gives $zJ' = -0.63$ cm^{-1}, and $D = 1.6$ cm^{-1}. The zJ' and D values are too large compared with the reported ones[26] and the expected ones for the $Cr(O)_6$ chromophore type complex, respectively. Thus, this treatment may not be appropriate for this case. As the other possiblity, the intramolecular coupling associated with the intermolecular interactions is taken into consideration in terms of the spin Hamitonian $\boldsymbol{H} = -2J\mathbf{S}_1 \cdot \mathbf{S}_2 + g\beta\mathbf{S}_z H - 2zJ' \langle S_z \rangle \mathbf{S}_z$ according to the following equation of the molar susceptibility of the $Cr^{III}-Gd^{III}$ ($S_{Cr} = {}^3/_2$, $S_{Gd} = {}^7/_2$) system:

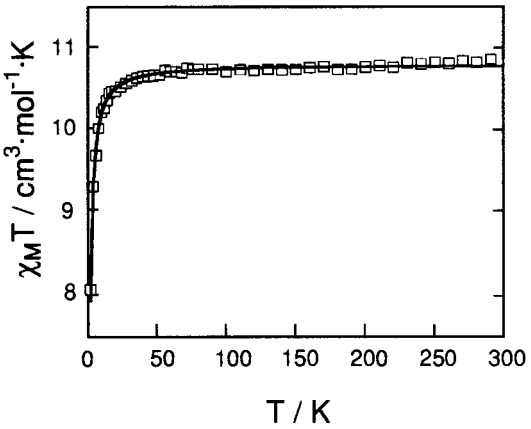

Figure 5. Plots of the $\chi_M T$ versus T for complex **2**. The solid line corresponds to the best data fits (see text).

$$\chi_M = Ng^2\beta^2 F(J,T)/[kT - 2zJ'F(J,T)] \qquad (1)$$

where $F(J,T) = [110 + 60\exp(10x) + 26\exp(18x) + 10\exp(24x)\}]/[\{11 + 9\exp(10x) + 7\exp(18x) + 5\exp(24x)]$, $x = -J/kT$, and the other symbols have their usual meanings. A good fit to the experimental data is obtained for $J = +0.02$ cm^{-1}, $g = 2.10$, $zJ' = -0.04$ cm^{-1} with the agreement factor $R = \Sigma[(\chi_M)_{obs} - (\chi_M)_{calc}]^2/\Sigma(\chi_M)_{obs}$ equal to 1×10^{-5}. Although this gives a better agreement factor than that estimated assuming $zJ' = 0$ which fits to eq 1 with $J = -0.09$ cm^{-1} and $g = 2.10$ with R equal to 1.6×10^{-4} as shown in Figure 5, the former result appears less meaningful in view of the requirement for the molecular field approximation that J is much larger than zJ'.[1b,27] The latter treatment neglecting zJ' points to a very weak antiferromagnetic intramolecular interaction between the Cr(III) and Gd(III). Most of the transition $metal^{II}\cdots Gd^{III}$ dinuclear complexes with few exceptions such as $Cu(oxae)Gd(phen)_2(ClO_4)_3$[8c] exhibit ferromagnetic coupling, which is accounted for by the theoretical consideration[6] based on a 3d → 5d charge transfer. A negligible ferromagnetic contribution to the magnetic interaction in the $Cr^{III}-Gd^{III}$ complex may result from the longer Cr···Gd distance than those of the hitherto reported $M^{II}-O-Gd$ type complexes (M = Cu, Ni, VO^{2+})[5-9,12] and/or the larger energy costs for charge-transfer transitions from the 3d orbital of a Cr(III) ion to the 5d orbital of a Gd(III) ion (i.e., the $Cr^{IV}-Gd^{II}$ excited state from the $Cr^{III}-Gd^{III}$ ground state) than those of M(II) ions in view of the difference in oxidation state; both of them result in decrease of ferromagnetic contribution.

(b) Energy Transfer. In general, Eu(III) and Tb(III) complexes exhibit a characteristic sharp luminescence.[28] How-

(26) (a) Carlin, R. L.; Burriel, R. *Phys. Rev. B* **1983**, 27, 3012. (b) Merabet, K. E.; Carlin, R. L. *Inorg. Chem.* **1989**, *28*, 4125.
(27) O'Connor, C. J. *Prog. Inorg. Chem.* **1982**, 29, 203.
(28) (a) Stein, G.; Würzberg, E. *J. Chem. Phys.* **1975**, *62*, 208. (b) Horrocks, W. DeW., Jr.; Albin, M. *Prog. Inorg. Chem.* **1984**, *31*, 1. (c) Lawrence, R. G.; Jones, C. J.; Kresinski, R. A. *J. Chem. Soc., Dalton Trans.* **1996**, 501.

Table 7. Phosphorescence Lifetimes (τ) for the Complexes

complex	λ_{ex}/nm	λ_{em}/nm	T/K	τ_{Ln}/ms	τ_{Cr}/ms
1 (Eu)	330	618[a]	293/77	n.o.[d]	
	395	618	293/77	n.o.	
	580	618	293/77	n.o.	
3 (Tb)	330	545[b]	293/77	n.o.	
	490	545	293/77	n.o.	
	330	780[c]	77		0.13
	550	780	77		0.11
4 (Yb)	330	780	77		n.o.[d]
	550	780	77		n.o.
5 (Lu)	330	780	77		0.19
	550	780	77		0.19

[a] Transition of $^5D_0 \rightarrow {}^7F_2$ for Eu(III). [b] Transition of $^5D_4 \rightarrow {}^7F_5$ for Tb(III). [c] Transition of $^2E \rightarrow {}^4A_2$ for Cr(III). [d] n.o. means "could not be observed".

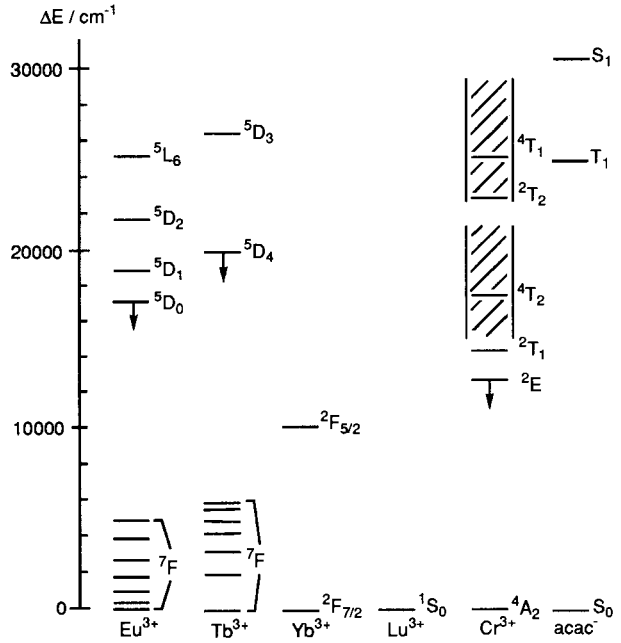

Figure 6. Energy level diagram showing 4f states of Ln(III), 3d states of Cr(III), and ligand levels of $acac^-$. The arrows indicate emission levels of Eu(III), Tb(III), and Cr(III).

ever, the microcrystalline samples of **1** and **3** did not show sharp emission bands at either room temperature or 77 K, when the exciting wavelengths were 330 nm (CT and/or intraligand transition due to the coordinated acac) and 395 nm [$^7F_0 \rightarrow {}^5L_6$ for Eu(III)], 580 nm [$^7F_0 \rightarrow {}^5D_0$ for Eu(III)], or 490 nm [$^7F_6 \rightarrow {}^5D_4$ for Tb(III)]. Therefore, the emission lifetimes of Eu(III) and Tb(III) could not be measured (Table 7). Since the ligand field absorption band envelope for the Cr(III) chromophore overlap with the spectral range of the narrow emissions of Eu(III) and Tb(III), the efficient quenching occurs in the Ln(III) luminescence resulting from the resonance between the Ln(III) excited levels and the broad ligand field state of the Cr(III) ion (Figure 6). This quenching behavior is compared with that of the double complex salts $[CrL_x][Ln(dipic)_3]$ [L = am(m)ines, Ln = Eu, Tb].[29]

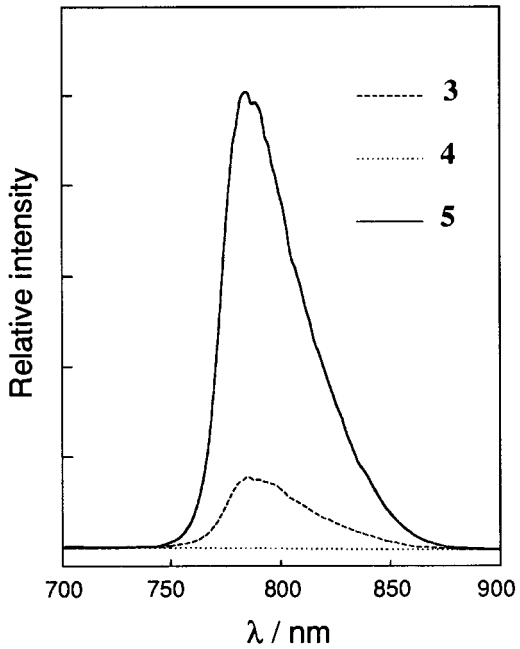

Figure 7. Cr(III) emission spectra of complexes **3**, **4**, and **5** at 77 K, where the exciting wavelength is 330 nm.

Emission spectra arising from the ^2E excited state in Cr(III) ion of complexes **3**, **4**, and **5** are observed at 77 K as shown in Figure 7. The peak positions of **3** (784 nm) and **5** (780 nm) are almost similar to that of $Na[Cr(acac)_2(ox)]\cdot H_2O$ (775 nm), but **4** gives no emission band in this region. Although the peak positions are a little different between **3** and **5**, both the relative intensity and phosphorescence lifetimes (Table 7) of **3** are smaller than those of **5**. These facts show that the quenching of emission originating from the ^2E excited state of Cr(III) results from the energy transfer to the Ln(III) possessing the low-lying energy levels (Figure 6): (i) complete quenching due to the energy transfer to the $^2F_{5/2}$ level of Yb(III) in **4** because of the relative small energy gap (ca. 2500 cm^{-1}); (ii) incomplete quenching due to the energy transfer to the $^7F_0$ of Tb(III) in **3** because of the large energy gap ca. 7000 cm^{-1}; (iii) no quenching in **5** with lack of low-lying energy levels for Lu(III).

Conclusions

The results described here have shown that (i) a series of the discrete 3d−4f heterodinuclear complexes are synthesized by a relatively simple method using a "complex ligand", (ii) the metal−metal interactions in the new complexes between the Cr(III) and Ln(III) are very weak in magnetic interaction but are strong from the viewpoint of energy transfer, where the degree of emission quenching depends on the energy gap of the excited levels in two metal centers.

Acknowledgment. This research was supported by a Grant in Aid for Scientific Research (No.06453049) from the Ministry of Education, Science and Culture.

Supporting Information Available: One X-ray crystallographic file, in CIF format, is available on the Internet only. Access information is given on any current masthead page.

IC971568K

(29) Brayshaw, P. A.; Bünzli, J.-C. G.; Froidevaux, P.; Harrowfield, J. M.; Kim, Y.; Sobolev, A. N. *Inorg. Chem.* **1995**, *34*, 2068.